Influence of phase-locked loop aggregation on the dynamic aggregation of wind farm strings with heterogeneous parameters

Taul, Mads Graungaard; Wang, Xiongfei; Davari, Pooya; Blaabjerg, Frede

Published in:
IET Energy Systems Integration

DOI (link to publication from Publisher):
10.1049/esi2.12011

Publication date:
2021

Document Version
Publisher's PDF, also known as Version of record

Received: 4 September 2020 | Revised: 29 October 2020 | Accepted: 9 November 2020

IET Energy Systems Integration

DOI: 10.1049/esi2.12011

ORIGINAL RESEARCH PAPER

Influence of phase-locked loop aggregation on the dynamic aggregation of wind farm strings with heterogeneous parameters

Mads Graungaard Taul | **Xiongfei Wang** | **Pooya Davari** | **Frede Blaabjerg**

Department of Energy Technology, Aalborg University, Aalborg, Denmark

Correspondence

Mads Graungaard Taul, Department of Energy Technology, Aalborg University, Aalborg, Denmark.
Email: mads@graungaard.dk

Funding information

VillumFonden, Grant/Award Number: 00016591

Abstract

Offshore wind farms are cornerstone solutions for enabling large-scale integration of renewable energy. Due to the large number of wind turbines in a wind farm, each with their individual complex control structure, a detailed time-domain model for analysis of wind farms is impractical from a computational burden perspective. Accordingly, aggregated models have been presented to reduce the computation time. Despite the high activity in aggregated modelling of wind farms, dynamic aggregation considering heterogeneous converter controllers and filter parameters, including different phase-locked loop (PLL) parameters have not been discussed previously. To remedy this issue, this study proposes an aggregated structure-preserving model of a wind farm string where all converters have heterogeneous parameters. The proposed model is verified by simulations against a detailed numerical model of the wind farm string, showing its accuracy in preserving the wind farm string dynamics under a severe grid fault with different short-circuit ratios and PLL parameters. Through a comparison of four different PLL aggregation methods under the considered case studies, it is found that the PLL aggregation has a negligible influence on the aggregated response and, hence, the particular aggregation method employed is not of great importance.

1 | INTRODUCTION

When transitioning towards renewable-based power generation, offshore wind farms are key enabling technologies for large-scale integration of renewable energy [1]. Offshore wind power plants (WPP) typically include more than one hundred individual wind turbines, where each turbine consists of a high-order dynamical model [2]. When analyzing the behaviour of the WPP, detailed time-domain models are accurate in capturing the dynamical response of the system. However, due to the large number of turbines and their complex individual structure, a detailed simulation model including all wind turbines is not practical from a computational burden perspective [3]. E.g., the detailed model of the WPP studied in [4] uses 3436 differential equations to describe the system. To decrease this highly impractical computational burden, equivalent and aggregated representations of the WPP are typically performed.

The aggregated modelling of WPP has been studied extensively in the past [3,5], and is often used to analyze the impact of a wind farm on the external power system [6]. Wind farm aggregation typically includes an aggregated representation of the wind turbine converters, an equivalent simplified model for the collector system cable impedances, and an aggregated representation of the incoming wind speeds [7,8]. The wind turbines are often aggregated as single-machine or multimachine equivalents, where clustering of the multimachine equivalent can be accomplished in numerous ways, including *K*-means clustering [9], multi-objective optimization algorithm [10], support vector clustering [11], a simple clustering based on grouping of wind speeds [12], or clustering through coherency equivalence [13,14].

In general, aggregated models for the wind turbine converter use the full-order dynamics, i.e., a structure-preserving aggregation, where the filter and controller parameters are aggregated based on the injected power of each converter [15–19]. In [16], the aggregation is only performed on the generator-side converter and the dynamics of the grid-side converter are not considered. An equivalent structure-preserving model

is proposed for a microgrid consisting of grid-following and grid-forming converters in [17]. In [18,19], an aggregation method based on impedance distance clustering on a generalized network framework is proposed. Common to all the above structure-preserving aggregation methods is that homogeneous phase-locked loop (PLL) parameters are considered and that PLL aggregation of the grid-side converter is not discussed. Such an assumption may not be justified in real large-scale applications. Thus, how to select the PLL parameters of the aggregated converter remain unanswered. Furthermore, the importance of PLL aggregation and how the PLL aggregation impacts the overall aggregated response has not been studied previously. To address this, the structure-preserving aggregation of a wind farm string is extended in this work to converters having heterogeneous controller and filter parameters, including different PLL parameters. Four different methods for PLL aggregation are compared and their impacts on the wind farm string aggregation are analyzed. For the analysis performed, it is shown that the developed aggregated model is highly accurate in preserving the point of common coupling (PCC) dynamics and that the particular PLL aggregation method employed has a negligible impact on the overall aggregated response.

The study is structured as follows: The Anholt 400 MW WPP under study is presented in Section 2. Aggregation of the collector system impedances and the dynamic aggregation of the string converters are presented in Section 3. Here, four different PLL aggregation methods are presented including a method based on the weighted averaging of the point of synchronization (POS) voltages of the string converters. The presented structure-preserving aggregated model of the studied wind farm string is verified by simulations in Section 4, where the aggregated model is verified under different short-circuit ratios (SCRs) and PLL bandwidths. In Section 5, the four PLL aggregation methods are compared and their influence on the overall aggregated model is outlined. Finally, the results and findings of this work are concluded in Section 6.

2 | DESCRIPTION OF STUDIED WIND FARM

In this study, the 400 MW Anholt offshore WPP is considered, as shown in Figure 1. The Anholt WPP consists of 111 3.6 MW wind turbines and it is located approximately 20 km out of the eastern coast in Denmark [20]. The physical configuration of the turbines and the medium-voltage collector system is depicted in Figure 1. For this study, a string with nine converters is under study, as shown in Figure 1.

The collector cable separating all the nine converters has a distance of 600 m [21]. These lengths, including the cable data from [22] (2XS(FL)2YRAA 18/30(36) kV), are used to calculate the impedance values for the cable Π-model of the collector system in Figure 1. The data used for the export submarine and land cable can be found in [23], Table 49, and in [24], Table 28, respectively. Both cables use aluminum 800 mm^2 conductors. A 25 km three-core submarine cable is used offshore, whereas three 59.6 km single-core cables laid in flat formation are used on land [25]. The values for the cable impedances are listed in Table 1. The transformers connected to the export cables have an impedance of 0.05 pu with $X/R = 20$ and the shunt reactors can absorb up to 120 MVAr. The wind-turbine transformers have a 0.1 pu impedance with $X/R = 10$. For the subsequent analysis, the impedance of the export cables is scaled based on the desired capacity of the WPP during the test. i.e., since only one string is under study, the

TABLE 1 Cable data used for Anholt WPP

Cable type	R (mΩ/km)	L (mH/km)	C (μF/km)
Collector: 150 mm^2	124	0.39	0.19
Collector: 240 mm^2	75.4	0.36	0.23
Collector: 500 mm^2	36.6	0.32	0.32
Submarine cable	33.75	0.17	0.4
Land cable	33.75	0.56	0.17

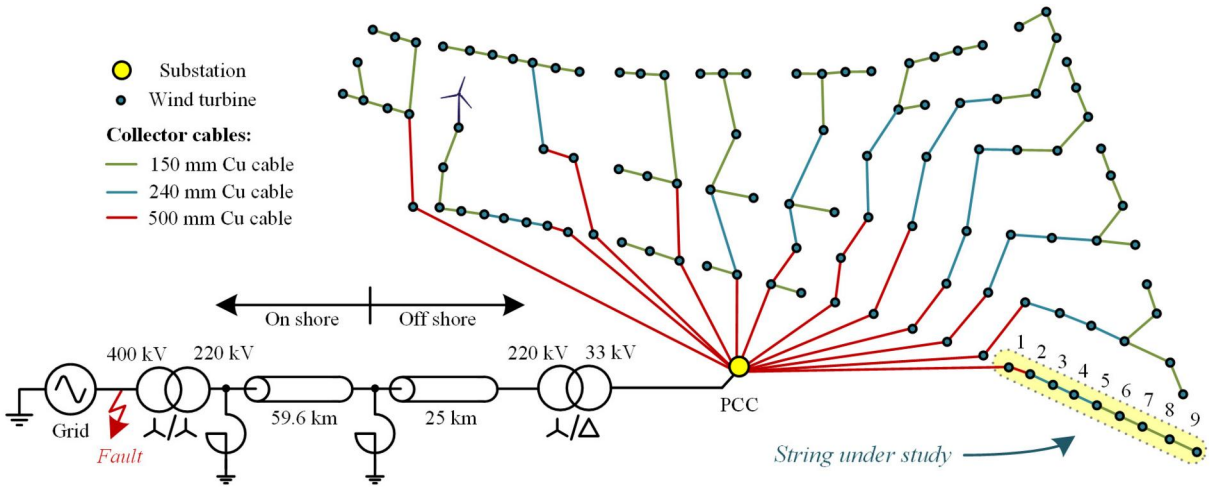

FIGURE 1 The physical layout of Anholt 400 MW offshore WPP with the electrical export system and connections [20,25]. One wind farm string with nine wind turbines is under study, as highlighted, where the string converter numbers are also denoted

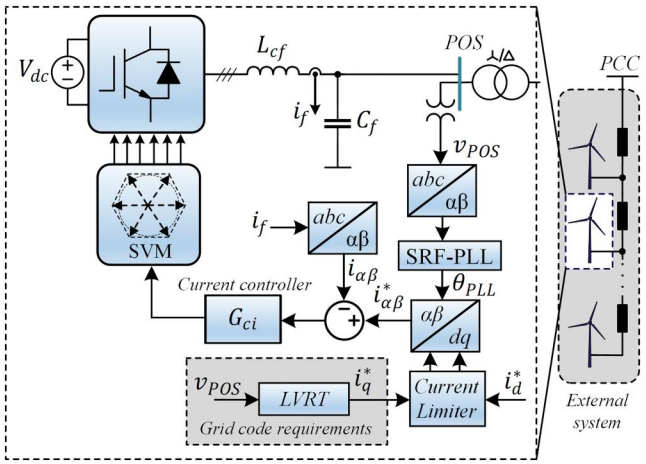

FIGURE 2 Detailed view of the grid-following control structure used to model each wind turbine in the wind farm string. POS: Point of synchronization and LVRT: Low-voltage ride-through.

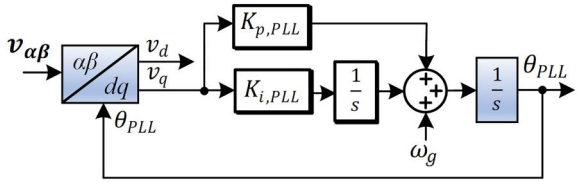

FIGURE 3 Detailed view of the SRF-PLL used for the grid-following control in Figure 2.

impedance of the export cable is increased by approximately 12, to get the same SCR as when the WPP is operating with all 12 strings.

The wind turbines are of Type IV with a back-to-back converter configuration, which facilitates decoupled analysis between the generator-side converter and the grid-side converter [26]. Hence, only the grid-side converters and their aggregation are considered in this study. Also, the operating point of each converter is assumed constant for this analysis since the harvested power from the wind turbines changes much slower than the dynamics associated with the grid-side string converters and the disturbed power system.

All grid-side converters in the wind farm string are modelled as grid-following converters with the control structure shown in Figure 2. The POS voltage at the low-voltage side of the wind-turbine transformer is considered for synchronization using a synchronous-reference frame (SRF) PLL . A detailed view of the SRF-PLL used for synchronization is shown in Figure 3. The current reference for active power is manually set, whereas the reactive current component is based on the low-voltage ride-through (LVRT) grid-code requirements in [27]. For each converter, a constant dc-link is considered with a voltage of $V_{dc} = 1250$ V.

3 | DYNAMIC AGGREGATION

For the structure-preserving dynamically aggregated model, an equivalent system is being developed with the aim of preserving the voltages and currents at the PCC. This is divided into an equivalent of the collector system impedance and an aggregated representation of the converter filters and controller parameters.

3.1 | Collector system equivalencing

A detailed view of the wind farm collector grid system is shown in Figure 4, which is used to derive the collector system equivalent impedance. The collector system impedances are usually equivalenced based on the preservation of the apparent power loss [2,7,28,29]. For the following, it is assumed that the phase difference between the injected converter currents and the POS voltages is small. This implies that only the magnitudes of the injected currents and the voltages at their respective connections can be considered for the aggregation. This assumption is approximately valid in practice since the collector cable impedances are usually much smaller than the park transformer and export cables. With this, the total apparent power loss in the collector system can be expressed as:

$$S_{tot} = \sum_{i=1}^{n} \left(\left(\sum_{j=i}^{n} I_j \right)^2 Z_{c,i} + Z_{tl} I_i^2 \right), \tag{1}$$

where I_i is the current magnitude of the i^{th} converter. This is then compared to an equivalent representation of the system as:

$$S_{tot} = I_{eq}^2 Z_{eq} = Z_{eq} \left(\sum_{i=1}^{n} I_i \right)^2. \tag{2}$$

Equaling the two expressions for the apparent power, the equivalent collector impedance can be isolated as:

$$Z_{eq} = \frac{\sum_{i=1}^{n} \left(\left(\sum_{j=i}^{n} I_j \right)^2 Z_{c,i} + Z_{tl} I_i^2 \right)}{\sum_{i=1}^{n} I_i^2}. \tag{3}$$

The collector impedances ($Z_{c,i}$) in Equation (3) only contain the resistance and inductive reactance of the collector cable. Also, Z_{eq} can be separated into the equivalent resistance, reactance, and transformer leakage reactance as:

$$R_{eq} = \Re \left[\frac{\sum_{i=1}^{n} \left(\sum_{j=i}^{n} I_j \right)^2 Z_{c,i}}{\sum_{i=1}^{n} I_i^2} \right], \tag{4}$$

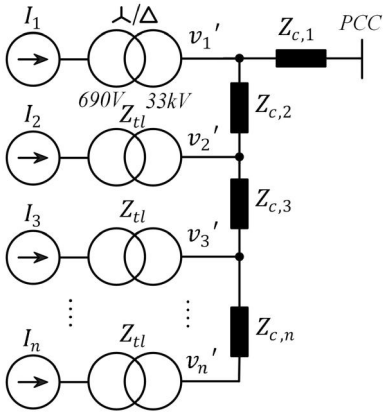

FIGURE 4 Detailed view of wind farm collector grid system where each grid-side grid-following converter is represented as a current source. PCC: Point of common coupling. See Figure 1 for details on the external view of the PCC

$$X_{eq} = \Im\left[\frac{\sum_{i=1}^{n}\left(\sum_{j=i}^{n} I_j\right)^2 Z_{c,i}}{\sum_{i=1}^{n} I_i^2}\right], \tag{5}$$

$$X_{tl,eq} = \frac{\sum_{i=1}^{n} Z_{tl} I_i^2}{\sum_{i=1}^{n} I_i^2}. \tag{6}$$

The collector cable capacitances are equivalenced in the following. The voltage at the high-voltage side of the wind-turbine transformer of the k^{th} turbine in Figure 4 is:

$$v_k' = v_{PCC} + \sum_{i=1}^{k}\left(\sum_{j=i}^{n} I_j Z_{c,i}\right). \tag{7}$$

The total apparent power loss in the shunt capacitances is:

$$S_{tot,C} = \sum_{i=1}^{n} C_i\left(|v_i'|^2 + |v_{i-1}'|^2\right), \tag{8}$$

where C_i is the shunt capacitance placed at each end of the Π-model of the i^{th} collector cable and $v_0' = v_{PCC}$. The equivalent apparent power loss of the shunt capacitance is:

$$S_{eq,C} = C_{eq}\left(|v_{eq}'|^2 + |v_{PCC}|^2\right), \tag{9}$$

where the weighted averaged voltage at the high-voltage wind-turbine transformer side in the equivalent system is [8]:

$$v_{eq}' = \frac{\sum_{i=1}^{n} v_i' S_i}{\sum_{i=1}^{n} S_i}. \tag{10}$$

Comparing Equations (8) and (9), the equivalent shunt capacitance can be expressed as:

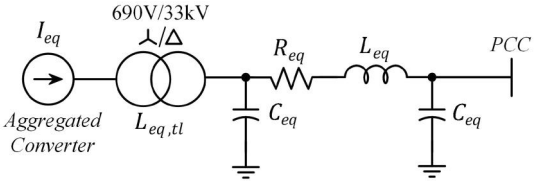

FIGURE 5 Structure of equivalent impedances for string collector system to where the aggregated converter is connected

$$C_{eq} = \frac{\sum_{i=1}^{n} C_i\left(|v_i'|^2 + |v_{i-1}'|^2\right)}{|v_{eq}'|^2 + |v_{PCC}|^2}. \tag{11}$$

When calculating the equivalent shunt capacitance, the PCC voltage is taken as a reference, where $|v_{PCC}|$ is 1 pu and $\angle v_{PCC} = 0°$. Thereby, the equivalent collector system can be represented as shown in Figure 5. With the derived equivalent impedance, the aggregated model of the string converter is presented.

3.2 | Dynamic aggregation of converter control and filter

As previously mentioned, due to the decoupling between the machine-side and grid-side converter for a Type IV wind turbine, only the operating point of the wind turbine is needed for the grid-side aggregation. Due to the time-scale separation between the fast dynamics of the studied ac-side large-signal disturbances and the slow dynamics of the wind speed and wind-turbine drive-train, the machine-side electrical and mechanical dynamics can be ignored in the aggregation.

Since the n string converters have different controller parameters, loading levels, and passive filter components, i.e., heterogeneous parameters, the aggregated equivalent converter needs to take this into account. A per-unit scaling parameter is defined to reflect the relative nominal current contribution of each converter against the total injected current as discussed in [17].

$$\lambda_i = \frac{I_i}{\sum_{j=1}^{n} I_j}. \tag{12}$$

Then, the aggregated parameters for the converter output filter and the current controller are calculated as a weighted average as:

$$L_{cf,agg} = \frac{1}{n}\sum_{i=1}^{n} \lambda_i L_{cf,i}, \tag{13}$$

$$L_{gf,agg} = \frac{1}{n}\sum_{i=1}^{n} \lambda_i L_{gf,i}, \tag{14}$$

$$C_{f,agg} = n\sum_{i=1}^{n} \lambda_i C_{f,i}, \tag{15}$$

$$K_{p,agg} = \frac{1}{n}\sum_{i=1}^{n} \lambda_i K_{p,i}, \tag{16}$$

$$K_{i,agg} = \frac{1}{n}\sum_{i=1}^{n} \lambda_i K_{i,i}. \tag{17}$$

The reference current for the aggregated string converter is:

$$I_{eq}^{ref} = \sum_{i=1}^{n} I_{d,i}^{ref} + j \sum_{i=1}^{n} I_{q,i}^{ref}. \tag{18}$$

Aggregation of Phase-Locked Loop Dynamics contrary to prior state-of-the-art studies where the paralleled converters are considered to have homogeneous PLL parameters, this study presents and compares different aggregation techniques for the synchronization dynamics as well. Instead of presenting a weighted averaged of the parameters based on the converter power, the POS voltage is adopted, since the PLL is a voltage-based synchronization method. Using the expression for v_k', the voltage at the low-voltage side of the wind-turbine transformer can be expressed as:

$$v_k = v_{PCC} + \sum_{i=1}^{k} \left(\sum_{j=i}^{n} I_j Z_{c,i} \right) + I_i Z_{tl}. \tag{19}$$

This is the POS voltage shown in Figure 2 for the k^{th} converter to where the PLL (see Figure 3) is connected. The aggregated PLL parameters are then obtained based on the weighted average of the POS voltages and associated PLL parameters for the n converters, given as:

$$K_{p,PLL,agg} = \frac{\sum_{i=1}^{n} K_{p,PLL,i} |v_i|}{\sum_{i=1}^{n} |v_i|}, \tag{20}$$

$$K_{i,PLL,agg} = \frac{\sum_{i=1}^{n} K_{i,PLL,i} |v_i|}{\sum_{i=1}^{n} |v_i|}. \tag{21}$$

To assess the influence and importance of the PLL aggregation procedure, the above proposed method (later denoted as *Weighted POS*) is compared to three other simpler PLL aggregation methods. These include a method where the aggregated PLL parameters are selected from the slowest PLL in the string, denoted as *Min*, a method based on the fastest PLL in the string, denoted as *Max*, and a method which uses an average of the PLL parameters in the string, denoted as *Average*.

4 | SIMULATION AND MODEL VERIFICATION

The developed aggregated model is compared to a detailed full-order averaged model of the WPP string. Each converter is adopting the control structure in Figure 2. This includes the aggregated converter model where the aggregated filter and controller parameters are determined from Equations (13) (14) (15) (16) (17) (18) (19) (20) (21). For heterogeneous operation each string converter has different values for the filter parameters, loading level, and controller parameters as listed in Table 2. The heterogeneous parameters for this case study are selected for model verification and do not necessarily represent typical values for a WPP.

TABLE 2 Heterogeneous parameters for simulation

Symbol	Description	Value	Variation
L_{cf}	Converter-side inductor	50 μH	± 20% random
C_f	Converter filter capacitor	2 mF	± 10% random
I_i	Converter current injection	0.7–1 pu	Linearly from 1 to 9
$f_{BW,CC}$	Current control bandwidth	250–500 Hz	Linearly from 9 to 1
t_{rise}	Rise time of PLLs	0.02 ms	± 40% random
$Z_{ext,8\%}$	Z_{ext} for 8% capacity	Z_{ext}	-
$Z_{ext,50\%}$	Z_{ext} for 50% capacity	$6.25Z_{ext}$	-
$Z_{ext,100\%}$	Z_{ext} for 100% capacity	$12Z_{ext}$	-

For the converter filter parameters each converter has nominal values of $L_{cf} = 50$ μH and $C_f = 2$ mF, to which a variation of ± 20% for the inductance and ± 10% for the capacitance is randomly added to each filter component of the n string converters. The loading levels of the converters are linearly distributed in the range 0.75–1 pu to take into account wake effects [30]. Likewise, the inner current controllers are tuned with a bandwidth between 500 Hz and 250 Hz. The bandwidth is linearly distributed between the nine converters where converter 1 has a bandwidth of 500 Hz and converter 9 has a bandwidth of 250 Hz. For the PLL parameters of the string converters, a nominal design where the PLL damping is $\zeta = 0.707$ and the rise time of 20 ms is selected. For heterogeneous PLL parameters, a random ± 40% variation is added to the nominal designed PLL rise time (t_{rise}). Using the randomly selected rise times, the PLL parameters are selected as:

$$K_{p,PLL,i} = \frac{2\zeta \cdot 1.8}{t_{rise,i} U}, \quad K_{i,PLL,i} = \frac{1}{U} \left(\frac{1.8}{t_{rise,i}} \right)^2, \tag{22}$$

where $U = 690\sqrt{2/3}$ $[V]$. The string of the Anholt WPP is simulated using MATLABs Simulink and PLECS blockset, which are compared to the response of the aggregated model. A 50% load decrease and increase are simulated for the system as shown in Figure 6. Also, a comparison is made during a grid voltage phase jump as seen in Figure 7. As can be seen from both test cases, a strong match between the two models is observed.

In order to further verify the dynamic behaviour, a three-phase symmetrical grid fault is simulated where the voltage at the fault location drops to 0.3 pu. During the fault, the string converters are switched to inject 1 pu of reactive current to support the local voltages. When the fault is cleared, the converters are again prioritizing active current injection based on their initial available power setpoints.

The magnitudes of the voltages and currents at the PCC, and the instantaneous power for the proposed model and the

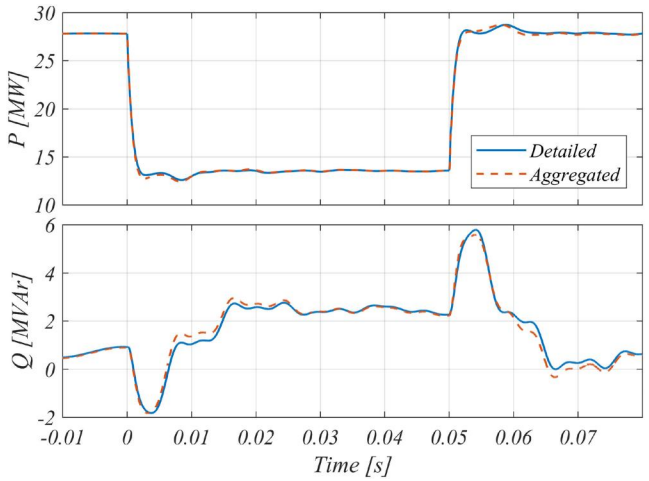

FIGURE 6 Comparison for active and reactive power at PCC between detailed simulation model of nine converters and the aggregated model using the *Weighted POS* given in Equations (20) and (21) for PLL aggregation during a 50% load decrease and increase, occurring at 0 *s* and 0.05 *s*, respectively

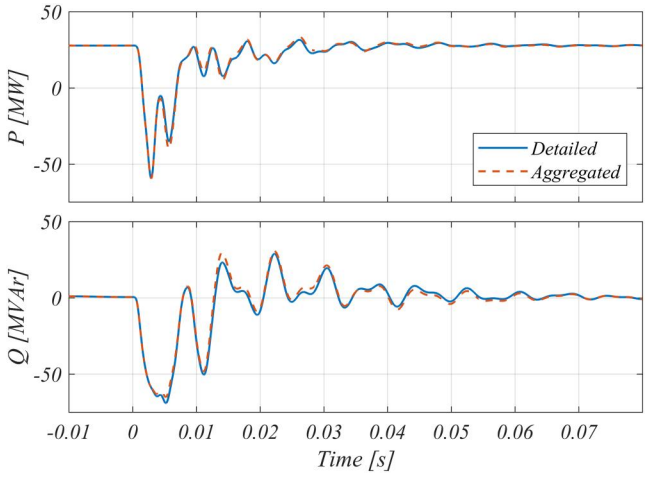

FIGURE 7 Comparison for active and reactive power at PCC between detailed simulation model of nine converters and the aggregated model using the *Weighted POS* given in Equations (20) and (21) for PLL aggregation during a –60° phase jump, occurring in the grid voltage at 0 *s*

detailed simulation model are shown in Figure 8 for three different export cable impedances (Z_{ext}) as listed in Table 2. In Figure 8a, the actual datasheet values are used for the export cables, and since only one string is simulated, this represents a low in-feed case of 8% capacity of the WPP. As can be seen, the aggregated model exactly captures the dynamics on the PCC. To simulate a scenario where 50% of the WPP capacity is generated, the export cables are increased 6.25 times in value to give the same SCR as for the actual WPP during this capacity. This is shown in Figure 8b, where still a good reproduction of the aggregated model is observed. Finally, a 100% in-feed capacity with a $SCR = 5$ is simulated in Figure 8c where the external impedance is increased 12 times from the datasheet values. Here, the aggregated model produces an accurate behaviour of the WPP response, where a larger damping is observed in the detailed system, as the fault recovery oscillation decays faster.

To test the PLL aggregation, which is based on the weighted average of the converters' POS voltages, a test scenario where the collector cables are increased 10 times in length compared to the real system configuration is conducted. This is done to see the impact when the POS voltages of the converters are less coupled. To that end, the centre bandwidth of the PLLs used for the converters is increased to 60 Hz (t_{rise} = 10 ms) to analyze the aggregation accuracy of the model. The results for this are shown in Figure 9, where a strong match between the aggregated and detailed model is observed, despite the increased collector impedance between the converters.

As demonstrated in Figures 8 and 9, the aggregated model closely matches the detailed simulation model for the entire WPP operating range.

Regarding computational requirements, the time needed to compute a 1-second simulation with a 0.2 s fault condition for the full-order averaged model and the aggregated model is compared. The simulations are performed on a Lenovo ThinkPad with 8 GB of RAM, a 2.80 GHz Intel Core i7-7600U processor, and a Windows 10 64-bit operating system. The models are implemented in MATLABs Simulink version 2017a using PLECS blockset version 4.1.1. The simulation model is solved using the variable step size autosolver in Simulink with maximum step size and relative tolerance of 1e-4 and 1e-3, respectively. The computational time needed is 85.14 s and 24.75 s for the detailed and aggregated model, respectively. This verifies that in addition to the high accuracy of the aggregated model, the computational requirements used for simulation can be significantly reduced.

5 | INFLUENCE OF DIFFERENT PLL AGGREGATION METHODS

As verified in the previous section, the aggregated model well preserves the PCC dynamics including the *Weighted POS* PLL aggregation method from Equations (20) and (21). However, whether the dynamic aggregation is sensitive to the PLL aggregation is unknown. To address this, the aggregated model using the four mentioned PLL aggregation methods from Section 3 is analyzed with the same PLL parameter variation as described in the previous section. The comparison of the different PLL aggregation methods to the detailed model during a symmetrical fault with the original Z_{ext} is shown in Figure 10. As can be noticed, all methods provide a nearly exact preservation of the PCC dynamics. This clearly indicates that the PLL aggregation has a negligible influence on the dynamic aggregated response. To that end, the same case but with 20 times the collector grid impedance was simulation. Again, the PLL aggregation method is observed to have a negligible influence on the aggregated model.

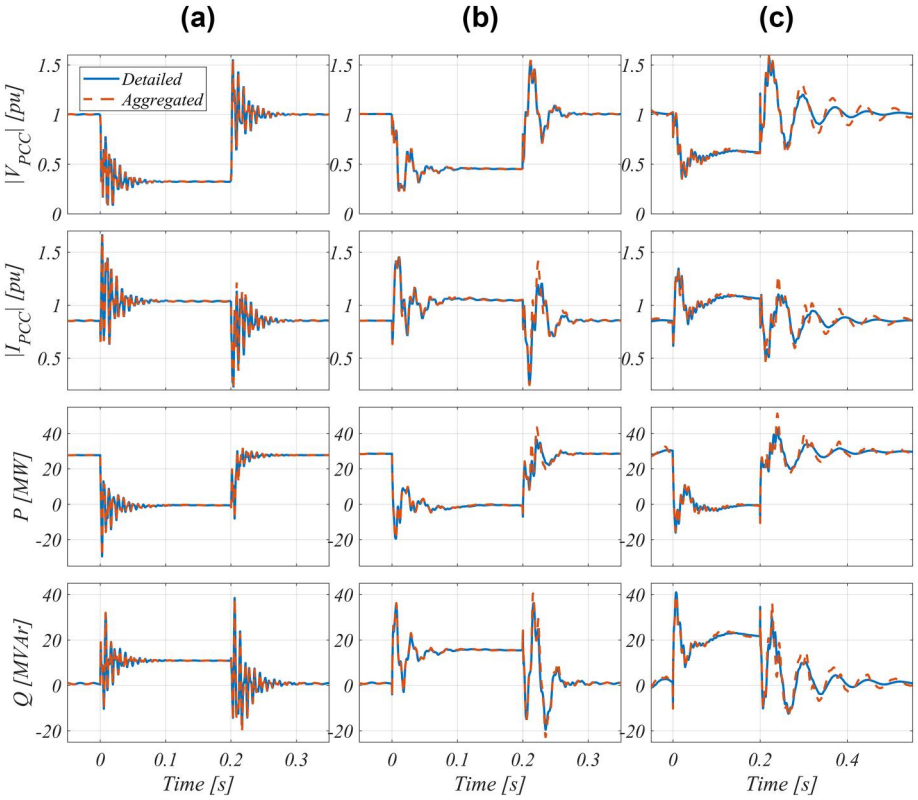

FIGURE 8 Comparison between detailed simulation model of nine converters and the aggregated model using the *Weighted POS* in Equations (20) and (21) for PLL aggregation during a three-phase symmetrical fault where the fault voltage magnitude drops to 0.3 pu. (a): Original values for export cable, which is equal to 8% capacity ($SCR = 60$), (b): 50% capacity ($SCR = 10$), and (c): 100% capacity ($SCR = 5$).

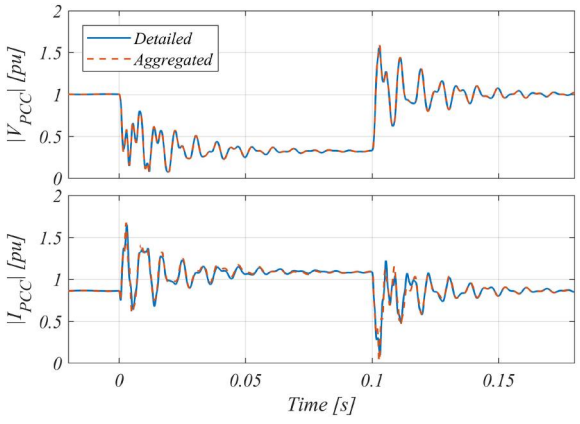

FIGURE 9 Comparison between detailed simulation model of nine converters and the aggregated model using the *Weighted POS* in Equations (20) and (21) for PLL aggregation during a three-phase symmetrical fault where the fault voltage magnitude drops to 0.3 pu for 100 ms. The PLL bandwidth is centred around 60 Hz ($t_{rise} = 10$ ms) and the collector cable impedance is 10 times the original value. Original values for external cable impedances with $SCR = 60$

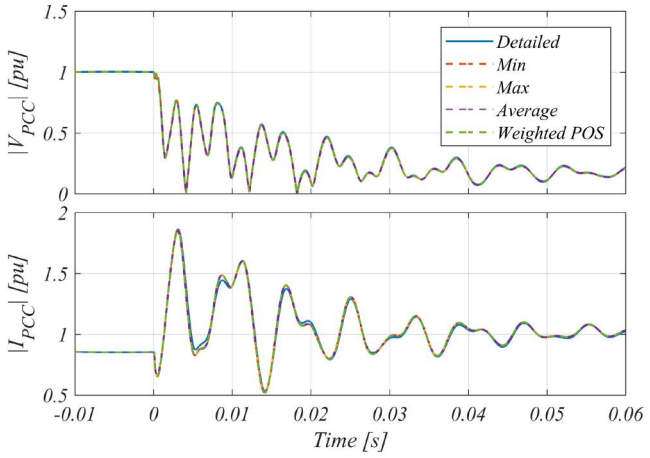

FIGURE 10 Comparison between different phase-locked loop aggregation methods during a three-phase symmetrical fault where the fault voltage magnitude drops to 0.3 pu and original Z_{ext} ($SCR = 60$). The response is shown during fault occurrence happening at 0 *s*.

A similar comparison is made in Figure 11 with $SCR = 5$. This is shown for the fault occurrence in Figure 11a and for the fault clearing in Figure 11b. It can be observed that the initial response is highly determined by the perturbed network, whereas the different methods for PLL aggregation start to have some impact afterwards. Despite, the *Weighted POS* and *Average* aggregation methods provide the most accurate responses, the discrepancy observed when employing different PLL aggregation methods is small. The absolute error in the PCC voltage and current magnitudes is shown for the different

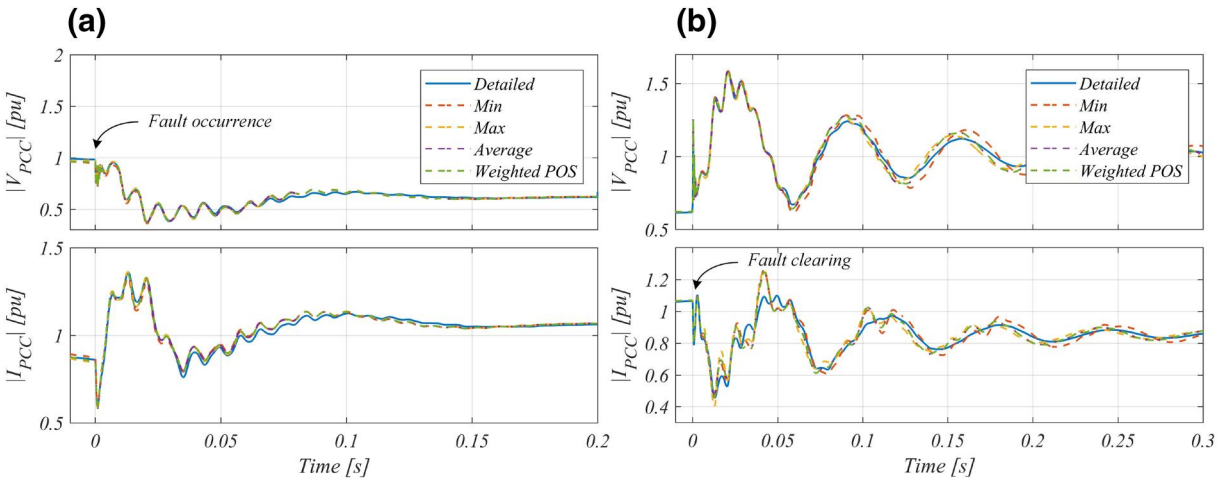

FIGURE 11 Comparison between different phase-locked loop aggregation methods during a three-phase symmetrical fault where the fault voltage magnitude drops to 0.3 pu and $SCR = 5$: (a) response during fault occurrence and (b) response during fault clearing. SCR, short-circuit ratio

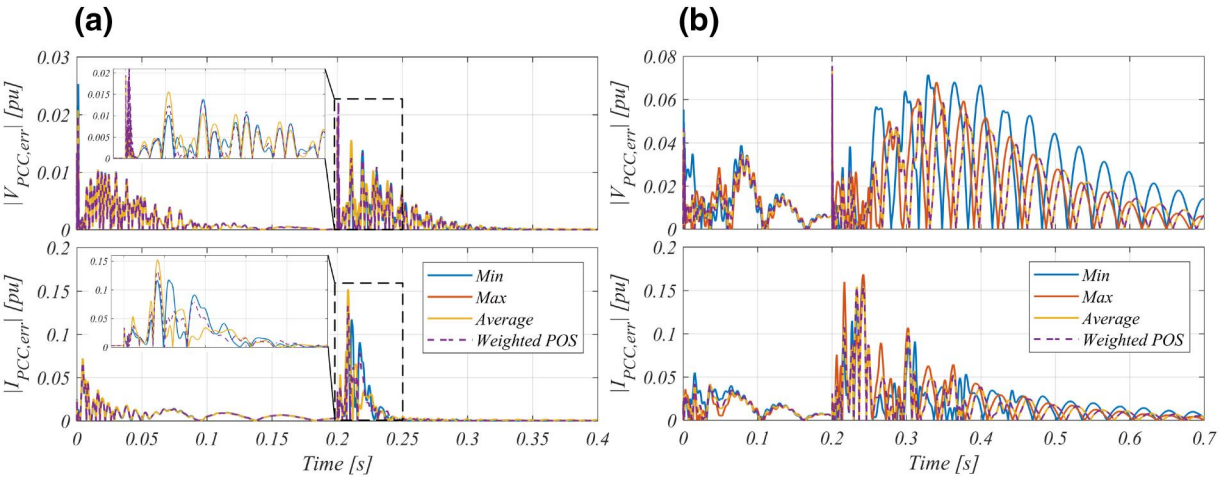

FIGURE 12 Comparison between absolute per-unit error for the point of common coupling voltage and current using different phase-locked loop aggregation methods during a three-phase symmetrical fault where the fault voltage magnitude drops to 0.3 pu, (a) $SCR = 60$ and (b) $SCR = 5$. The fault occurs at $t = 0$ s and it is cleared at $t = 0.2$ s. SCR, short-circuit ratio

TABLE 3 Average error in magnitude of PCC voltage and current

PLL aggregation method	avg($\lvert V_{PCC,err} \rvert$)	avg($\lvert I_{PCC,err} \rvert$)
$SCR = 60$		
Weighted POS	0.001 pu	0.0049 pu
Min	0.0014 pu	0.0065 pu
Max	0.0013 pu	0.0064 pu
Average	0.0011 pu	0.0054 pu
$SCR = 5$		
Weighted POS	0.0182 pu	0.0218 pu
Min	0.0229 pu	0.0243 pu
Max	0.0186 pu	0.0232 pu
Average	0.0169 pu	0.0203 pu

Abbreviations: PLL, phase-locked loop; POS, point of synchronization; SCR, short-circuit ratio.

TABLE 4 Oscillation frequency after fault recovery with $SCR = 5$

PLL aggregation method	Oscillating frequency (Hz)
Detailed model	15.41
Weighted POS	15.22
Min	14.73
Max	15.85
Average	15.53

methods for a $SCR = 60$ and a $SCR = 5$ in Figure 12a,b, respectively. At first, it is evident that the error increases with a decreased SCR. To that end, for the high SCR case, the difference between the PLL aggregation methods is negligible. For the case with $SCR = 5$, the difference is larger and the *Min* and *Max* aggregation methods provide the largest errors. Yet,

as mentioned above, the error difference between the methods is relatively minor.

The averaged error over the entire fault duration for the different methods for $SCR = 60$ and $SCR = 5$ is listed in Table 3. As can be seen, the *Weighted POS* and *Average* give the smallest errors.

To that end, the oscillating frequencies observed after fault recovery are recorded for the different methods, as listed in Table 4. Again, the *Weighted POS* provides the most accurate results, but with a relatively small difference compared to the other methods.

Accordingly, as anticipated, it can be concluded that the *Weighted POS* and *Average* methods provide the best results for the preservation of the PCC dynamics. However, as it has been analyzed, the particular PLL aggregation method used has a minor influence on the overall aggregated result for low SCR grids and a negligible influence under high SCR conditions. Hence, the PLL aggregation seems not of great importance for the overall dynamic aggregation.

6 | CONCLUSION

This work has proposed a structure-preserving dynamic aggregation method for a wind farm string. Different from previous studies, this model takes into account heterogeneous PLL parameters using a proposed PLL aggregation method and analyzes the influence of PLL aggregation on the overall dynamic aggregated model. The dynamic aggregated model is compared to a detailed model of a string with nine converters in the Anholt 400 MW wind farm. The proposed model shows a close agreement in preserving the PCC dynamics of the original system, which is verified for different SCRs within the capacity range of the real operating Anholt wind farm. Four different methods for PLL parameters aggregation are presented. Through a comprehensive comparison of the different PLL aggregation methods, it was observed that the difference between the four PLL aggregation methods is negligible under strong grid conditions and is minor during weak-grid conditions. Therefore, it is observed that the overall dynamic aggregated model is nearly independent of the PLL aggregation and, hence, the method used for PLL aggregation seems not of great importance. Future study includes investigating how the dc-link control may affect the findings presented here. In addition to this, the proposed aggregated model serves as a very feasible model to preserve the dynamics at the PCC within the wind farm operating area and may, therefore, be accurately employed for dynamic aggregation in large wind farms.

ACKNOWLEDGEMENT

This work was supported by the Reliable Power Electronics-Based Power System (REPEPS) project at the Department of Energy Technology, Aalborg University, as a part of the Villum Investigator Program funded by the Villum Foundation.

ORCID

Mads Graungaard Taul https://orcid.org/0000-0001-9584-1379

REFERENCES

1. Bresesti, P., et al.: Hvdc connection of offshore wind farms to the transmission system. IEEE Trans. Energy Conv. 22(1), 37–43 (2007)
2. Taul, M.G., et al.: Reduced-order and aggregated modeling of large-signal synchronization stability for multi-converter systems. IEEE J. Emerg. Sel. Topics Power Electron. 1–17 (2020). https://doi.org/10.1109/JESTPE.2020.3015293
3. Kunjumuhammed, L.P., et al.: The adequacy of the present practice in dynamic aggregated modeling of wind farm systems. IEEE Trans. Sust. Energy. 8(1), 23–32 (2017)
4. Linash, P., et al.: Electrical oscillations in wind farm systems: Analysis and insight based on detailed modeling. IEEE Trans. Sust. Energy. 7(1), 51–62 (2016)
5. Al-bayati, A.M.S., Mancilla-David, F., Domínguez-Garcíal, J.L.: Aggregated models of wind farms: Current methods and future trends. In: 2016 North American power symposium (NAPS), Denver, CO, USA. pp. 1–6 (2016)
6. Altin, M., et al.: Aggregated wind power plant models consisting of IEC wind turbine models. In: 2015 IEEE Eindhoven PowerTech, Einhoven. pp. 1–5 (2015)
7. Martínez-Turégano, J., et al.: Model aggregation of large wind farms for dynamic studies. In: IECON 2017 - 43rd annual conference of the IEEE Industrial Electronics Society, Beijing, China. pp. 316–321 (Oct 2017)
8. Gupta, A.P., Mohapatra, A., Singh, S.N.: Apparent power loss based equivalent model of wind farm collector system. In: 2018 20th National power systems conference (NPSC), Tiruchirappalli, India. pp. 1–6 (2018)
9. Fang, R., et al.: Application of gray relational analysis to k-means clustering for dynamic equivalent modeling of wind farm. Int. J. Hydrog. Energy. 42(31), 20154–20163 (2017)
10. Wang, P., et al.: Improved wind farm aggregated modeling method for large-scale power system stability studies. IEEE Trans. Power Syst. 33(6), 6332–6342 (2018)
11. Teng, W., et al.: An improved support vector clustering approach to dynamic aggregation of large wind farms. CSEE J Power Energy Syst. 5(2), 215–223 (2019)
12. Li, W., et al.: A practical equivalent method for DFIG wind farms. IEEE Trans. Sust. Energy. 9(2), 610–620 (2018)
13. Zha, X., et al.: Dynamic aggregation modeling of grid-connected inverters using hamilton's-action-based coherent equivalence. IEEE Trans. Ind. Electron. 66(8), 6437–6448 (2019)
14. Ali, H.R., et al.: Model order reduction of wind farms: Linear approach. IEEE Trans. Sust. Energy. 10(3), 1194–1205 (2019)
15. Vijayshankar, S., et al.: Reduced-order aggregate dynamical model for wind farms. In: 2019 American control conference (ACC), Philadelphia, PA, USA. pp. 5464–5471 (2019)
16. Dai, J., Tang, Y., Wang, Y.: Aggregation frequency response modeling for wind farms with frequency support capabilities. In: 2019 IEEE power energy society general meeting (PESGM), Atlanta, GA, USA. pp. 1–5 (2019)
17. Shuai, Z., et al.: Dynamic equivalent modeling for multi-microgrid based on structure preservation method. IEEE Trans. Smart Grid. 10(4), 3929–3942 (2019)
18. Purba, V., et al.: Dynamic aggregation of grid-tied three-phase inverters. IEEE Trans. Power Syst. 35(2), 1520–1530 (2020)
19. Purba, V., et al.: Network-cognizant model reduction of grid-tied three-phase inverters. In: 2017 55th Annual Allerton Conference On Communication, Control, and Computing, Allerton, Monticello, IL, USA. pp. 157–164 (2017)
20. Kocewiak, L.H., et al.: Resonance damping in array cable systems by wind turbine active filtering in large offshore wind power plants. IET Renew. Power Gener. 11(7), 1069–1077 (2017)
21. Ørsted, D.K.: Anholt offshore wind farm (2019). http://dise.org.pl/dania2019/AnholtOffshoreWindFarm.pdf. Accessed September 1, 2020

22. Nexans: Submarine power cables (2008). https://www.nexans.com/Germany/group/doc/en/NEX_Submarine_neu.pdf. Accessed September 1, 2020
23. ABB.: Xlpe submarine cable systems attachment to xlpe land cable systems - user's guide. Tech. Rep. ABB's high voltage cable unit (2010)
24. ABB.: Xlpe land cable systems - user's guide. Tech. Rep. ABB's high voltage cable unit (2010)
25. Jensen, C.F.: Harmonic background amplification in long asymmetrical high voltage cable systems. Electr. Power Syst. Res. 160, 292–299 (2018)
26. Taul, M.G., et al.: An overview of assessment methods for synchronization stability of grid-connected converters under severe symmetrical grid faults. IEEE Trans. Power Electron. 34(10), 9655–9670 (2019)
27. VDE: VDE-AR-N 4110: Technical requirements for the connection and operation of customer installations to the medium-voltage network (TCC medium-voltage) (VDE (German Commission for Electrical Engineering, Electronic and IT) (2017)
28. Su, X., et al.: Comparison between the two equivalent methods of collector system for wind farms. In: 2015 International Conference on Estimation, Detection and Information Fusion (ICEDIF), Harbin, China. pp. 354–358 (2015)
29. Muljadi, E., et al.: Equivalencing the collector system of a large wind power plant. In: 2006 IEEE Power Engineering Society General Meeting, Montreal, Que., Canada. pp. 9 (2006)
30. Kuenzel, S., et al.: Impact of wakes on wind farm inertial response. IEEE Trans. Sust. Energy. 5(1), 237–245 (2014)

How to cite this article: Taul MG, Wang X, Davari P, Blaabjerg F. Influence of phase-locked loop aggregation on the dynamic aggregation of wind farm strings with heterogeneous parameters. *IET Energy Syst. Integr.* 2021;3:99–108. https://doi.org/10.1049/esi2.12011